Med Biol Eng Comput (2012) 50:1017–1023
DOI 10.1007/s11517-012-0919-3

ORIGINAL ARTICLE

Assessing spatial resolution versus sensitivity from laser speckle contrast imaging: application to frequency analysis

Stéphanie Bricq · Guillaume Mahé · David Rousseau · Anne Humeau-Heurtier · François Chapeau-Blondeau · Julio Rojas Varela · Pierre Abraham

Received: 3 November 2011 / Accepted: 13 May 2012 / Published online: 30 May 2012

Abstract For blood perfusion monitoring, laser speckle contrast (LSC) imaging is a recent non-contact technique that has the characteristic of delivering noise-like speckled images. To exploit LSC images for quantitative physiological measurements, we developed an approach that implements controlled spatial averaging to reduce the detrimental impact of the noise and improve measurement sensitivity. By this approach, spatial resolution and measurement sensitivity can be traded-off in a flexible way depending on the quantitative prospect of the study. As an application, detectability of the cardiac activity from LSC images of forearm using power spectrum analysis is studied through the construction of spatial activity maps offering a window on the blood flow perfusion and its regional distribution. Comparisons with results obtained with signals of laser Doppler flowmetry probes are performed.

S. Bricq (✉) · A. Humeau-Heurtier · F. Chapeau-Blondeau · J. Rojas Varela
Laboratoire d'Ingénierie des Systèmes Automatisés (LISA), Université d'Angers, 62 Avenue Notre Dame du Lac, 49000 Angers, France
e-mail: sbricq@esaip.org

S. Bricq
Groupe ESAIP, 18 rue du 8 mai 1945, BP 80022, 49180 St Barthélémy d'Anjou Cedex, France

G. Mahé · P. Abraham
Laboratoire de Physiologie et d'Explorations Vasculaires, UMR CNRS 6214-INSERM U 1083, Centre Hospitalier Universitaire d'Angers, 49933 Angers Cedex 09, France

D. Rousseau
Université de Lyon, CREATIS, CNRS, UMR 5220, INSERM, U630, Université de Lyon 1, INSA-Lyon, 69621 Villeurbanne, France

Keywords Microcirculation · Laser speckle contrast imaging · Laser Doppler flowmetry · Skin

1 Introduction

The cutaneous blood supply is a network of arterioles, arterial and venous capillaries, and venules. Skin microcirculation assessment is of interest in a number of clinical applications (ulcers, burns, skin grafts, Raynaud's syndrome, melanomas, drug development, cosmetology, diabetes, [9, 12, 16, 22]), and also in providing specific information concerning the cardiovascular system in general [6].

Two major techniques are currently used to monitor tissue perfusion: laser Doppler technology [laser Doppler flowmetry (LDF) and laser Doppler imager (LDI)] and laser speckle contrast (LSC) imaging. LDF is a contact method that provides a continuous non-invasive measure related with changes on microvascular perfusion (red blood cell concentration and velocity [2, 5, 10, 21]). LDF gives a temporal signal (1D information). To overcome contact measurements and spatial variability, LDI has been developed. LDI shows a good spatial resolution but a poor temporal resolution for most devices (especially when scanning large areas). Therefore, this makes difficult to compute frequency analyses.

LSC imagers have recently been developed [1]. LSC imaging shows good temporal and spatial resolution [15], and thus this technique is more suitable than LDI to compute frequency analyses. LSC imaging is intrinsically a 2D non-contact method, which exploits the spatial pattern of interference generated from diffusely backscattered laser light from the tissue. As a result, raw LSC images appear as very noise-like speckled images. For a given

task (such as the study of the post-occlusive reactive hyperaemia peak or a time–frequency analysis), it is possible to reduce the noise in LSC images by spatial averaging. This is obtained at the cost of a loss of spatial resolution. In this article, we propose a general approach to assess a sensitivity–resolution tradeoff with LSC imaging. To this purpose, we use the sensitivity of a single-point LDF probe as reference. Comparison between LDF signals and LSC images is a topic of current investigation. While LDF is described by a theory that is widely accepted and understood, the theoretical link between the speckle contrast and the tissue perfusion in LSC imagers is under development [4]. Another pragmatic way to assess the advantages and drawbacks of LDF signals and LSC images is to use standard clinical procedures as comparative frameworks. Such an approach has recently been developed for a post-occlusive reactive hyperaemia (in static conditions [13] or when the subject is moving [7]). In this article, we focus on the comparison of the detectability of the cardiac activity by analyzing the power spectrum of LSC images and LDF signals recorded on forearms [19, 20]. Rousseau et al. [13] studied the value of the cutaneous blood flow at rest and during post-occlusive reactive hyperaemia with different sizes of regions of interest, whereas in this manuscript, we perform a frequency analysis of the signal. This frequency analysis is applied to the detection of cardiac activity and can be seen as a preliminary step before performing other processings such as a wavelet analysis for the study of myogenic or neurogenic activities. Our objectives are to check if LSC imaging is more reliable than LDF technique for a frequency analysis in the context of detecting the cardiac rhythm and to study the influence of spatial averaging on the results.

2 Methods

Five male and female volunteers (aged 18 years or older) without known cardiovascular disease were recruited in this study. All microvascular tests were performed with subjects resting supine in a temperature-controlled room (23 ±1 °C). The LSC imager used has a 70 mW system (PeriCam PSI System®, Perimed, Sweden) and a laser wavelength of 785 nm. The sampling frequency was 18 Hz. Recordings were performed on the forearm. The distance between the laser head and skin surface was fixed at 20 cm, in the recommended range [8]. Images were stored on a computer and analyzed off-line. In addition, three single-point LDF probes (PF 408, Perimed, Sweden) connected to a laser Doppler flowmeter (PeriFlux PF5000, Perimed, Sweden, 780 nm laser diode) delivering a one-dimensional time recording were placed on the forearm as shown in Fig. 1. LDF signals were recorded with a sampling frequency of 20 Hz. In the LSC imager, the signal amplitudes backscattered from the skin were calculated using the manufacturer's software (PimSoft 1.2.2.0®, Perimed, Sweden) before being exported for the post-processing described below. The software expresses recorded values in arbitrary perfusion units. For each subject, a pressure cuff was placed on the subject's upper arm (proximal to the recording sites). The procedure included a 1 min baseline period, a 3 min period of cutaneous blood flow (CBF) occlusion (a cuff inflation at 200 mmHg), and a 6 min post-occlusion period. We analyzed the heart rate detectability during the baseline period at rest and during the occlusion period.

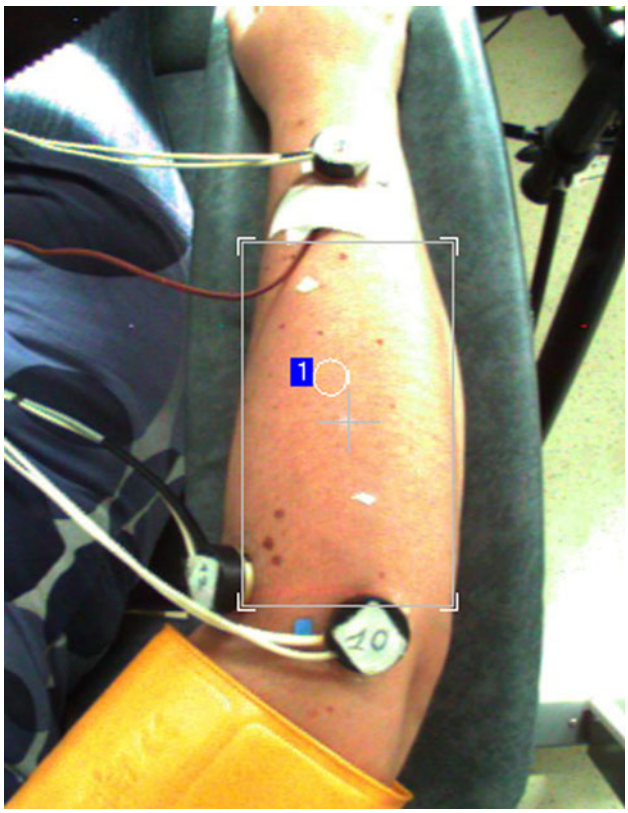

Fig. 1 View from the video camera included in the LSC imager

To compare the heart rate detectability in LDF signals and LSC images, we compute the periodogram $P(f)_{(x,y)}$ defined through a Fourier transform FT[.] in the time domain as

$$P(f)_{(x,y)} = |\mathrm{FT}[\mathrm{LSC}(x,y,t)](f)|^2 \quad (1)$$

for each temporal speckle signal $\mathrm{LSC}(x,y,t)$ located on pixel (x,y) of the LSC imager.

Then, we consider a spatial averaging over an $N \times N$ area of neighboring pixels, prior to the computation of the Fourier transform of the periodogram, according to

$$P_N(f)_{(x,y)} = \left| \mathrm{FT}\left[\frac{1}{N^2} \sum_{i=-(N-1)/2}^{(N-1)/2} \sum_{j=-(N-1)/2}^{(N-1)/2} \mathrm{LSC}(x-i, y-j, t) \right](f) \right|^2 \quad (2)$$

A drawback of the averaging or low-pass spatial filtering of Eq. (2) is that it reduces the spatial resolution of the image acquired with LSC imager. In such a situation, an optimal size for spatial averaging can result from a tradeoff between heart rate detectability and spatial resolution. To quantify this tradeoff, we define a signal-to-noise ratio (SNR) for the heart rate detectability. We consider the frequency band corresponding to cardiac activity from $f_{\min} = 0.6\,\mathrm{Hz}$ to $f_{\max} = 2\,\mathrm{Hz}$ [18]. In this frequency band, we compute the average and the maximal value of the periodogram $P_N(f)_{(x,y)}$ from Eq. (2). We therefore calculate the SNR S_N defined as

$$S_N = \frac{\max_f \left\{ P_N(f)_{(x,y)} \right\}}{\frac{1}{f_{\max} - f_{\min}} \int_{f_{\min}}^{f_{\max}} P_N(f)_{(x,y)} df} \quad (3)$$

3 Results

LSC imaging evaluates tissue perfusion for each pixel in the area visible in Fig. 1 at high temporal and high spatial resolutions (pixel size is approximately 0.46 × 0.46 mm^2 in Fig. 1). Figure 2a presents the laser speckle signal LSC(x, y, t) measured in one pixel (x, y) of the observed area of Fig. 1, and Fig. 2b presents signals obtained by spatial averaging over an area of size 9 × 9 pixels around this pixel. For comparison, Fig. 2c gives the LDF signal simultaneously recorded on the same forearm. To compare the heart rate detectability in LDF signals and LSC images, we compute the periodogram $P(f)_{(x,y)}$ [Eq. (1)] for each temporal speckle signal LSC(x, y, t) of Fig. 2 located on pixel (x, y) of the LSC imager. The results obtained are illustrated in Fig. 3 for one subject.

The cardiac activity gives a peak at the characteristic frequency around 1 Hz in Fig. 3. This peak is clearly visible in the periodogram calculated for the LDF signal, while it is not visible in the signal provided by only one pixel of the LSC imager. This is an effect of the strong noise masking the rhythmic cardiac activity in the speckle image. However, through spatial averaging over several neighboring pixels of the imager, there is a possibility of reducing the impact of the speckle noise, which is essentially independent from pixel to pixel, while reinforcing the rhythmic cardiac activity having a common origin from pixel to pixel.

After a spatial averaging over an $N \times N$ area of neighboring pixels, as observed in Fig. 3, the cardiac peak around 1 Hz also appears on the recordings of the LSC imager.

Then, we compute the SNR for LDF signals by following the procedure of Eq. (3). LDF signals are found to have an average SNR of 23 over the 5 tested volunteers. Average SNR over the three LDF probes is presented in Fig. 4 for each subject. Average SNR ranges from 17 to 36 with a standard deviation varying from 0.2 to 3.8.

Then, we consider four different areas of 39 × 39 pixels in the images acquired with LSC imager for the five tested volunteers. For each of these four areas, we focus on the central pixels. For these four pixels, we compute a spatial averaging over an $N \times N$ area of neighboring pixels (with N varying from 1 to 39). After this spatial averaging, we calculate the SNR S_N. Figure 5 presents the average SNR over the four areas for each subject for different values of N. Using Figs. 4 and 5, we can compare individually, for each subject, the results obtained with LDF and LSC imaging.

Average SNR increases with spatial averaging until it reaches a plateau. When the number of pixels N is higher than 21 (which corresponds to an area of 21 × 21 pixels or 93 mm^2), spatial averaging does not improve the SNR value. Thus, it is sufficient to compute the SNR on a 21 × 21 area of neighboring pixels.

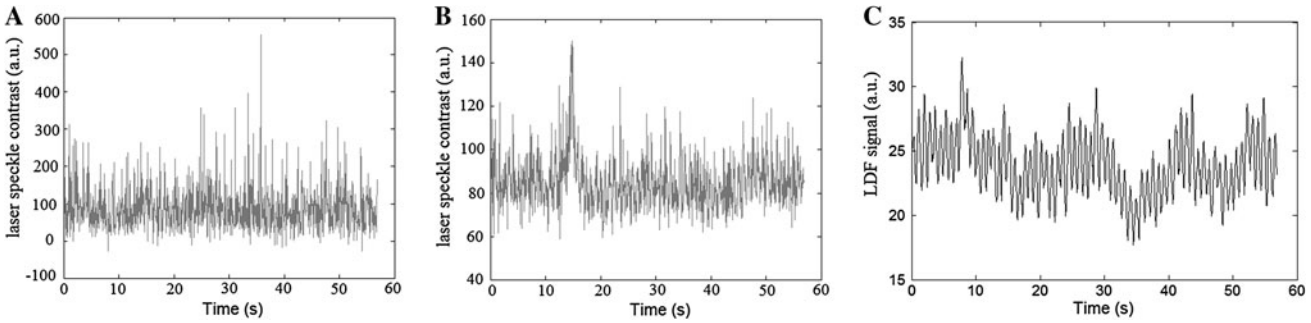

Fig. 2 **a** LSC(x, y, t) on one pixel (x, y) as a function of time t. **b** LSC(x, y, t) spatially averaged over an area of 9 × 9 pixels. **c** Corresponds to the LDF signal. Signals of all panels are simultaneously acquired on the same forearm at rest

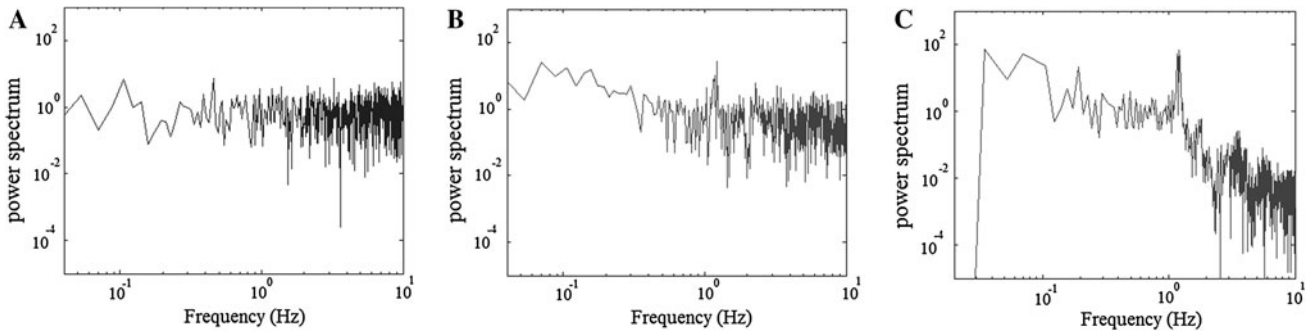

Fig. 3 Periodogram of signals in Fig. 1. **a** For LSC images with no spatial averaging, **b** with spatial averaging a 9 × 9 pixels area, and **c** for LDF signal

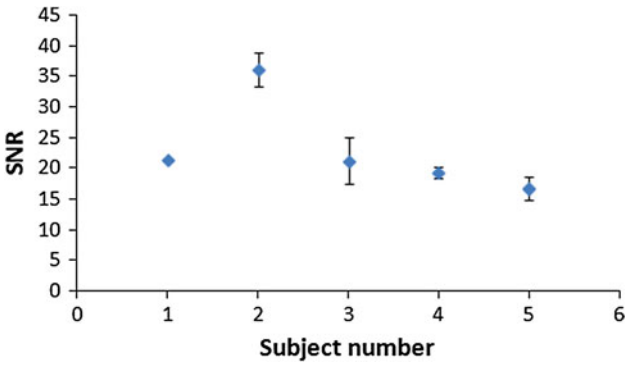

Fig. 4 Average SNR over the three LDF probes for the five tested volunteers

For this area size, average SNR ranges from 7 to 34 according to the subject with a standard deviation varying from 0.3 to 3.6. The mean SNR for LSC when averaging over 21 × 21 pixels was 16, which is lower than the average SNR obtained with LDF. Except for one subject, the obtained SNR is higher with the use of LDF probes than with LSC imaging. Furthermore, the standard deviation is quite similar for both techniques.

Once the sensitivity for detection of the cardiac peak is optimized at the desired level through an appropriate $N \times N$ size of the spatial averaging, the SNR of Eq. (3) can be calculated for each pixel from the LSC imager. This then provides the possibility of realizing spatial maps of the heart rate detectability, with a spatial resolution delimited by the choice of the $N \times N$ averaging area. Examples of such a map are shown in Fig. 6 with different $N \times N$ sizes of spatial averaging.

It is then observed that spatial patterns can be identified in the maps shown in Fig. 6. In order to verify the existence of plausible patterns and investigate their possible origins, we propose to follow the evolution of spatial maps as in Fig. 6 during an experiment of occlusion of the blood flow.

We calculate the SNR maps before occlusion, during occlusion and after occlusion. First, when no spatial averaging is realized, it is observed in Fig. 7a–c that there is no spatial structure visible in the calculated SNR maps. The only salient information in the maps of Fig. 7 is the overall reduction of the heart detectability during the occlusion.

Next, spatial averaging is performed to calculate the SNR maps as in Fig. 7d–f. It is observed on the maps in Fig. 7 that spatial patterns become visible before the occlusion, they disappear with the blood flow during occlusion, and they reappear after occlusion when the flow resumes.

This consistent evolution provides ground to the existence of significant spatial patterns present in the SNR maps of heart rate detectability. This raises the question of the physiological origin and interpretation of such patterns.

A possibility could be that they provide a window on the spatial organization of the microvascular network architecture and blood flow distribution.

4 Discussion

For LSC imaging which delivers very noise-like speckled images, we have proposed an approach to tradeoff spatial resolution and measurement sensitivity through controlled spatial averaging. The LSC images used for this study come from the PeriCam PSI System (Perimed, Sweden). The perfusion in a single measurement point has been calculated by the PeriCam system using a 3 × 3 window. Thus, the perfusion images that we processed have already been averaged by the PeriCam system. As an application in this paper, we have concentrated on the detectability of the heart as the physiological parameter of interest. We have quantified and compared the heart detectability with LSC imaging and LDF techniques. We have observed the existence of an optimal size of spatial averaging to obtain the highest SNR value with a minimal size of averaging. For this optimal size, LDF seems to remain the best technique for the heart detection in the major cases. This may suggest that LSC imaging is not the best technique to perform a frequency analysis. This frequency analysis is a

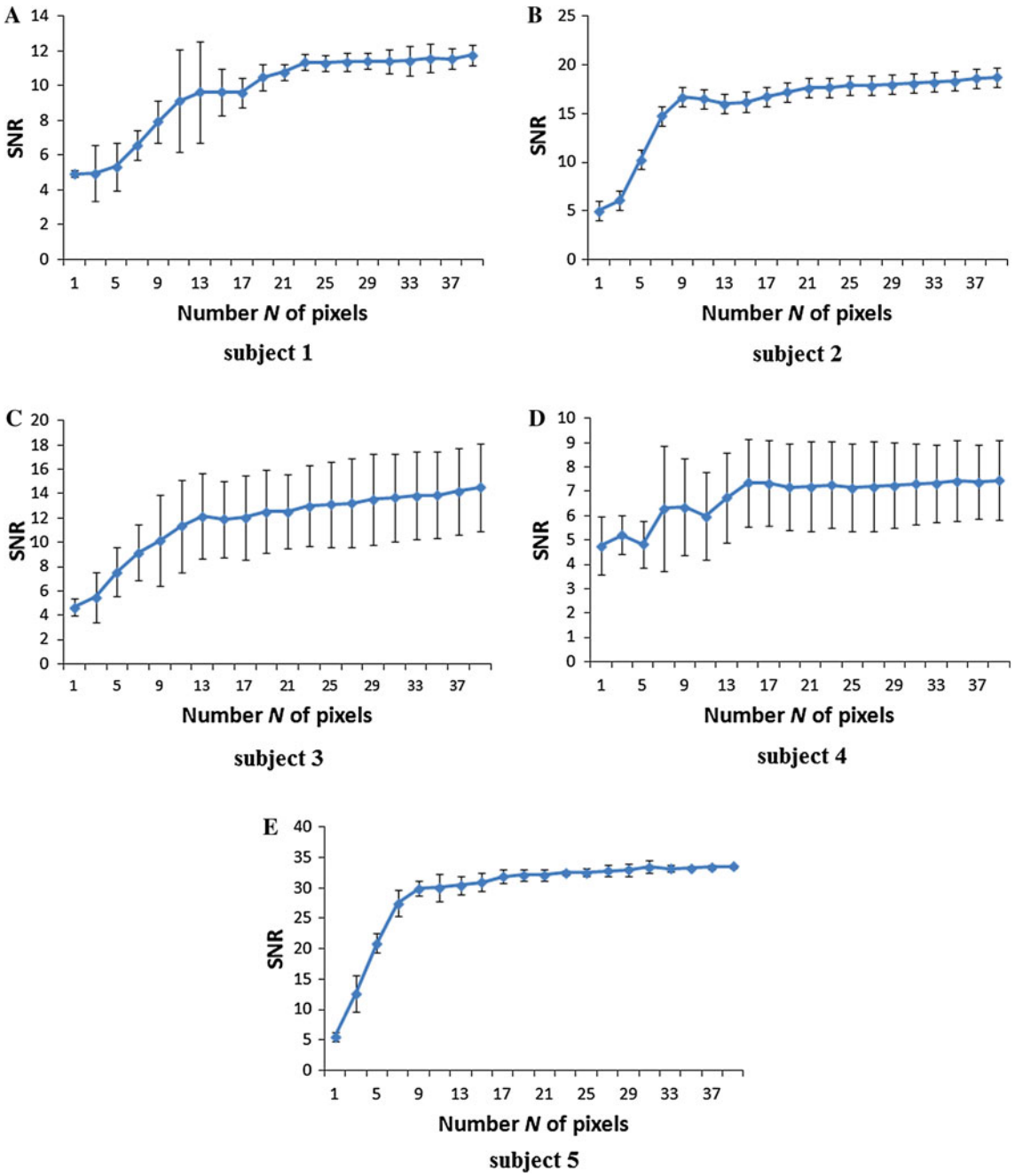

Fig. 5 Average SNR over the 4 areas computed on LSC images for the 5 tested volunteers for the SNR S_N from Eq. (3) for the cardiac peak detected in the periodogram spatially averaged over a $N \times N$ pixels area

first step for other processings, such as wavelet analysis, to study other physiological activities (neurogenic, myogenic [17]). However, LSC imaging has the advantage to be a non-invasive, non-contact technique for blood flow determination and, thanks to its imaging capability, this technique can be used to study structures of interest, such as burns [22] providing that the structure is larger than the optimal size of spatial averaging. Thus, with LSC imaging, we can plan to perform time–frequency or wavelet analyses on spatial structures, such as burns, which would be difficult with LDF because of contact or with LDI because of temporal resolution. Nevertheless, LDF and LSC imaging have different measurement depth (approximately 1 mm for the LDF and 300 μm for the LSC imager) [11]. Thus, these two techniques do not measure flux from the same skin layers. This may explain the SNR differences observed in this study. As the measurement depth is higher for the LDF, photons giving rise to the LDF signal will

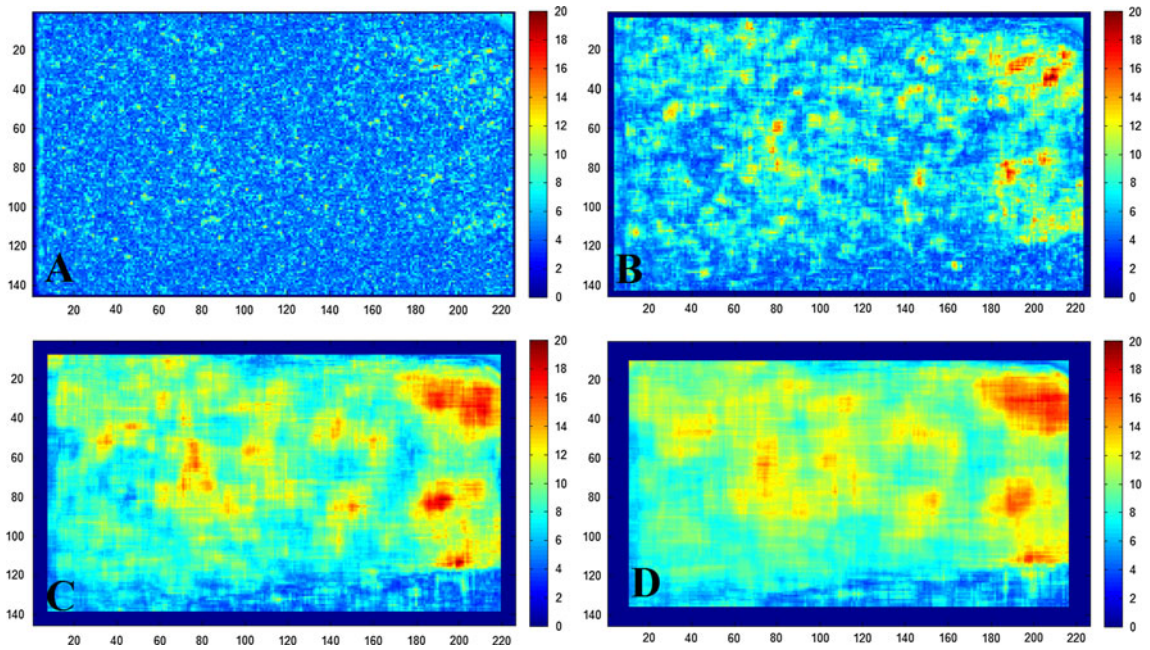

Fig. 6 Spatial map from LSC images for the SNR S_N of Eq. (3) calculated with various sizes $N \times N$ of the spatial averaging area: 3×3 (**a**), 7×7 (**b**), 15×15 (**c**), 21×21 (**d**) at rest

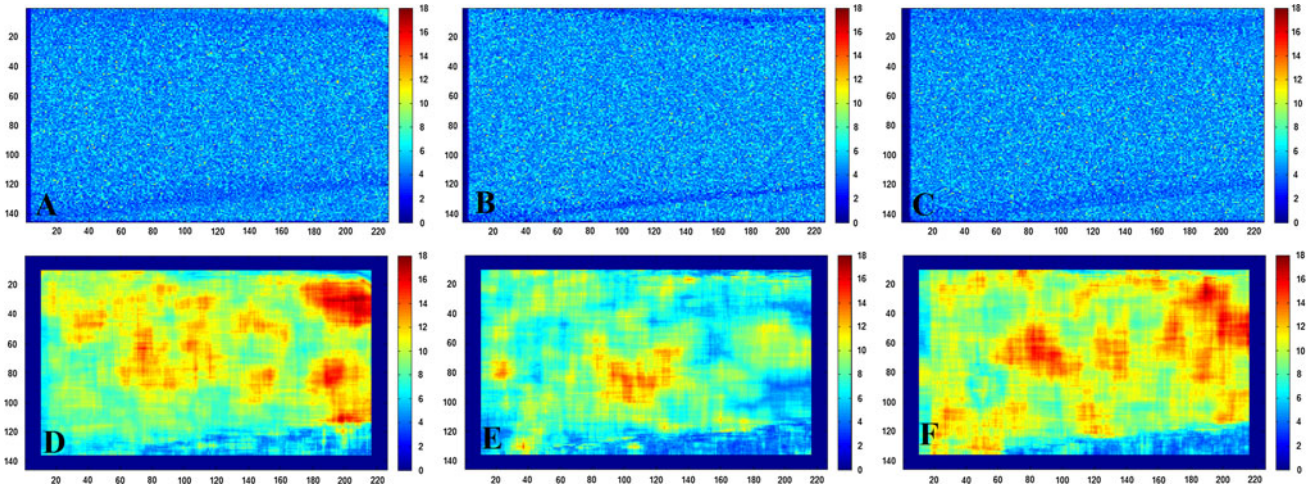

Fig. 7 Spatial map from LSC images for the SNR calculated for each pixel with no spatial average (*first line*), **a** at rest, **b** during occlusion, **c** at rest after occlusion, and with a spatial averaging area of 21×21 pixels (*second line*), **d** at rest, **e** during occlusion, **f** at rest after occlusion

encounter more vessels, which can explain that the SNR is higher with LDF than with LSC imaging.

Moreover, we have observed the possible existence of spatial patterns in the heart detectability. This spatial variability in the microvascular flow, as revealed by LSC imaging, could be at the origin of the known difficulty of securing reproducibility of the perfusion signal recorded from a single-point LDF probe [14, 15]. In this report, we considered heart detectability as the informational task of interest. Other information of clinical interest could be used as benchmark for the comparison of LSC images and LDF signals, in order to more fully appreciate how the imaging capabilities of LSC imagers can efficiently complement single-point LDF recording. For instance, post-occlusion relaxation hyperaemia could be used to generate spatial maps displaying the distribution of the physiological parameters that are commonly defined in the mathematical models describing such an experiment [3].

In conclusion, we compared the heart detectability with LSC imaging and LDF techniques using power spectrum analysis. The results obtained suggest that LDF is a better technique than LSC imaging to perform a frequency analysis. However, LSC imaging enables to perform time–

frequency or wavelet analyses on spatial structures such as burns.

References

1. Aizu Y, Asakura T (1991) Bio-speckle phenomena and their application to the evaluation of blood flow. Opt Laser Technol 23:205–219
2. Cai H, Rohman H, Larsson SE, Öberg PÅ (1996) Laser Doppler flowmetry: characteristics of a modified single-fibre technique. Med Biol Eng Comput 34(1):2–8
3. de Mul F, Blaauw J, Aarnoudse JG, Smit A, Rakhorst G (2005) A model for post-occlusive reactive hyperemia as measured with laser-Doppler perfusion monitoring. IEEE Trans Biomed Eng 52:184–190
4. Draijer M, Hondebrink E, Leeuwen T, Steenbergen W (2009) Review of laser speckle contrast techniques for visualizing tissue perfusion. Lasers Med Sci 24:639–651
5. Humeau A, Steenbergen W, Nilsson H, Strömberg T (2007) Laser Doppler perfusion monitoring and imaging: novel approaches. Med Biol Eng Comput 45(5):421–435
6. Humeau A, Buard B, Mahé G, Chapeau-Blondeau F, Rousseau D, Abraham P (2010) Multifractal analysis of heart rate variability and laser Doppler flowmetry fluctuations: comparison of results from different numerical methods. Phys Med Biol 55(20): 6279–6297
7. Mahé G, Rousseau P, Durand S, Bricq S, Leftheriotis G, Abraham P (2011) Laser speckle contrast imaging accurately measures blood flow over moving skin surfaces. Microvasc Res 81:183–188
8. Mahé G, Haj-Yassin F, Rousseau P, Humeau A, Durand S, Leftheriotis G, Abraham P (2011) Distance between laser head and skin does not influence skin blood flow values recorded by laser speckle imaging. Microvasc Res 82(3):439–442
9. Mahé G, Humeau-Heurtier A, Durand S, Leftheriotis G, Abraham P (2012) Assessment of skin microvascular function and dysfunction with laser speckle contrast imaging. Circ Cardiovasc Imaging 5(1):155–163
10. Nilsson G, Tenland T, Oberg P (1980) A new instrument for continuous measurement of tissue blood flow by light beating spectroscopy. IEEE Trans Biomed Eng 27:12–19
11. O'Doherty J, McNamara P, Clancy N, Enfield J, Leahy M (2009) Comparison of instruments for investigation of microcirculatory blood flow and red blood flow and red blood cell concentration. J Biomed Opt 14:034025
12. Rousseau P, Mahé G, Fromy B, Ducluzeau PH, Saumet JL, Abraham P (2009) Axon-reflex cutaneous vasodilatation is impaired in type 2 diabetic patients receiving chronic low-dose aspirin. Microvasc Res 78(2):218–223
13. Rousseau P, Mahé G, Haj-Yassin F, Durand S, Humeau A, Leftheriotis G, Abraham P (2011) Increasing the "region of interest" and "time of interest", both reduce the variability of blood flow measurements using laser speckle contrast imaging. Microvasc Res 82:1–4
14. Roustit M, Blaise S, Millet C, Cracowski JL (2010) Reproducibility and methodological issues of skin post-occlusive and thermal hyperemia assessed by single-point laser Doppler flowmetry. Microvasc Res 79:102–108
15. Roustit M, Millet C, Blaise S, Dufournet B, Cracowski JL (2010) Excellent reproducibility of laser speckle contrast imaging to assess skin microvascular reactivity. Microvasc Res 80:505–511
16. Roustit M, Blaise S, Millet C, Cracowski JL (2011) Impaired transient vasodilation and increased vasoconstriction to digital local cooling in primary Raynaud's phenomenon. Am J Physiol Heart Circ Physiol 301(2):324–330
17. Sheppard LW, Vuksanović V, McClintock PV, Stefanovska A (2011) Oscillatory dynamics of vasoconstriction and vasodilation identified by time-localized phase coherence. Phys Med Biol 56(12):3583–3601
18. Shiogai Y, Stefanovska A, McClintock PVE (2010) Nonlinear dynamics of cardiovascular ageing. Phys Rep 488:51–110
19. Stefanovska A, Lunchinsky D, Mc Clintock P (2001) Modelling couplings among the oscillators of the cardiovascular system. Physiol Meas 22:551–564
20. Stefanovska A, Lotric MB, Strle S, Haken H (2001) The cardiovascular system as coupled oscillators? Physiol Meas 22:535–550
21. Stern MD (1975) In vivo evaluation of microcirculation by coherent light scattering. Nature 254:56–58
22. Stewart C, Frank R, Forrester K, Tulip J, Lindsay R, Bray R (2005) Comparison of two laser-based methods for determination of burn scar perfusion: laser Doppler versus laser speckle imaging. Burns 31:744–752